

www.acsnano.org

# Design of Multifunctional Nanopore Using Polyampholyte Brush with Composition Gradient

Shiyi Qin, Kai Huang,\* and Igal Szleifer\*



Cite This: ACS Nano 2021, 15, 17678-17688



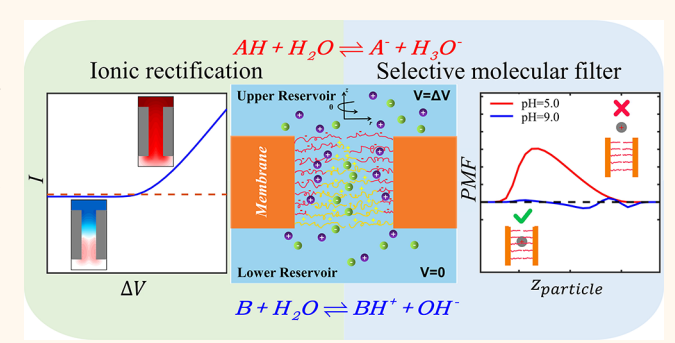
**ACCESS** 

III Metrics & More

Article Recommendations

S Supporting Information

ABSTRACT: Molecular organizations and charge patterns inside biological nanopores are optimized by evolution to enhance ionic and molecular transport. Inspired by the nuclear pore complex that employs asymmetrically arranged disordered proteins for its gating, we here design an artificial nanopore coated by an asymmetric polyampholyte brush as a model system to study the asymmetric mass transport under nanoconfinement. A nonequilibrium steady-state molecular theory is developed to account for the intricate charge regulation effect of the weak polyampholyte and to address the coupling between the polymer conformation and the external electric field. On the basis of this state-of-the-art theoretical method, we present a



comprehensive theoretical description of the stimuli-responsive structural behaviors and transport properties inside the nanopore with all molecular details considered. Our model demonstrates that by incorporating a gradient of pH sensitivity into the polymer coatings of the nanopore, a variety of asymmetric charge patterns and functional structures can be achieved, in a pH-responsive manner that allows for multiple functions to be implemented into the designed system. The asymmetric charge pattern inside the nanopore leads to an electrostatic trap for major current carriers, which turns the nanopore into an ionic rectifier with a rectification factor above 1000 at optimized pH and salt concentration. Our theory further predicts that the nanopore design behaves like a double-gated nanofluidic device with pH-triggered opening of the gates, which can serve as an ion pump and pH-responsive molecular filter. These results deepen our understanding of asymmetric transport in nanoconfined systems and provide guidelines for designing polymer-coated smart nanopores.

KEYWORDS: nanopore, molecular theory, weak polyampholyte, composition gradient, asymmetry

### **INTRODUCTION**

Biological pores and channels regulate the exchange of ions and molecules between cellular compartments. The outstanding selectivity and gating efficiency of these biological passageways are desired for a wide array of applications such as biosensing, 1-6 energy conversion, 7-10 and nanofiltration. 11-13 However, the understanding of biological nanopores is not complete due to the difficulty of experimental visualization of their dynamic ultrastructure. Growing research efforts have been devoted to developing artificial nanopores, especially biomimetic ones that allow for the transformation of biological functions into more robust man-made systems that are not limited to work at physiological conditions. 14-16 Artificial systems also provide an in vitro platform to investigate the gating mechanisms of biological nanopores, by either directly implementing biological components of interest 16,17 or employing synthetic coating materials 18-20 that emulate their biological analogs.

The advance in polymer synthesis has greatly expanded the material arsenal of functionalizing artificial nanopores. Stimuli-responsive polymers have been widely used as coating materials to enable the control of nanopores by a variety of environmental changes such as pH, <sup>19,21–23</sup> temperature, <sup>24–27</sup> light, <sup>28–30</sup> and membrane potential. <sup>31–33</sup> However, compared to the proteins that build highly structured biological nanopores, synthetic polymers are often trivial in composition and therefore not able to assemble into intricate structures. Nevertheless, many proteins have been realized to be

Received: June 29, 2021 Accepted: October 25, 2021 Published: October 28, 2021





intrinsically disordered like synthetic polymers. The fact that the largest biological nanopore—the nuclear pore complex (NPC)—relies heavily on disorder proteins to control the nucleocytoplasmic transport proves the potential of synthetic polymers as functional gating materials. Although the disordered proteins of the NPC lack fixed three-dimensional structure and bear more mutations than folded proteins, their well-defined anchoring positions and preserved sequence patterns suggest that the spatial distributions of functional motifs are not random inside the nuclear pore. Essentially, a number of disordered proteins of different amino-acid sequences are anchored to the NPC scaffold. It is interesting that the scaffold of the NPC has a quasi-symmetric shape, but the anchorage of disordered proteins is highly asymmetric. Our recent study indicates that the asymmetrically arranged disordered proteins of the NPC assemble into nanocompartments of distinct chemical properties inside the nuclear pore.<sup>34</sup>

Inspired by the NPC, here we explore the strategy of combining polymer anchorage control and sequence design to build a chemically heterogeneous nanoenvironment inside an artificial nanopore. We keep the shape of the nanopore symmetric and break the symmetry of the system by introducing a composition gradient into the coating polymers as a function of their anchoring positions along the axial direction of the nanopore. In particular, we use polyampholytes with a gradual change in monomer composition from predominantly basic monomer to mostly acidic monomer (see Figure 1). Such design allows the polymers to change their electrostatic and conformational status in a pH-responsive way and therefore potentializes the nanopore as smart ionic rectifier and molecular filter. To characterize the rectification property of the designed nanopore, we developed a nonequilibrium steady-state molecular theory that is able to account for the coupling between the polymer conformations and the external electric field, as well as the intricate interplay between the physical interactions and chemical reactions inside the nanopore. On the basis of this state-of-the-art approach, we found that the polyampholytes are capable of registering an electrostatic trap for the mobile counterions in a pHdependent manner, which provides a mechanistic explanation for the ionic rectification of the nanopore. With a delicate control over the depth of the electrostatic trap through pH and salt optimization, this nanopore design can produce rectification factors in excess of 1000. Our model also discovered a strong nonlinear effect in the combination between the intrinsic electrostatic potential at thermodynamic equilibrium and the applied biased potential that drives the system out of equilibrium, which creates significantly deeper and wider ionic traps than what are expected under the assumption of linear superposition. To evaluate the filtering performance of the nanopore, we calculated the free energy landscapes of various large cargoes translocating the pore. We show that the translocation barrier is sensitive to the charge of the cargo and responsive to external stimuli. The selectivity of the filter can be optimized by adjusting the grafting density of the polymer. Lastly, ion pumping can be realized based on the designed nanopore as the asymmetric polymer brush exhibits opposing gating behaviors at its two ends. The insight from this work could deepen our understanding of the role of asymmetry in a biomimetic system and guide the rational design of bioinspired nanodevices.

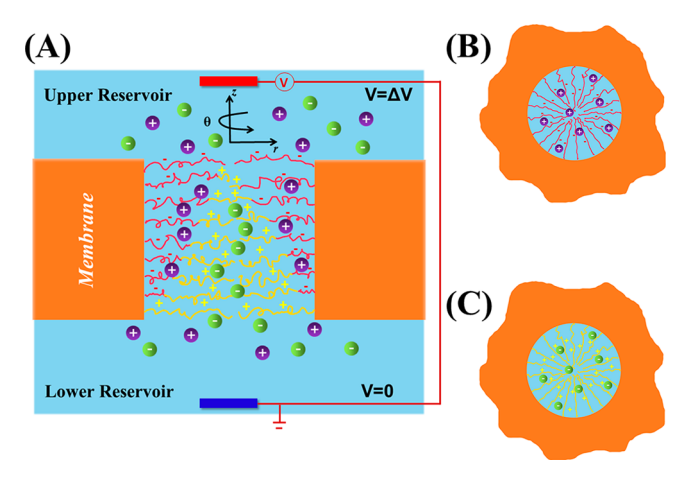


Figure 1. (A) Scheme of the nanopore system under study: a single cylindrical nanopore of length L = 42 nm and pore radius R = 6.5nm in a membrane connects two identical reservoir containing salt anions and cations, as well as protons and hydroxyl ions. The inner walls of the pore are modified by polyampholyte layers with a composition gradient. The bottom block (red) consists of acid monomers, and the top one (yellow) is composed of basic monomers. The dissociation constants  $(pK_a)$  of acid and basic monomers are set to be 6 and 8, respectively. Both kinds of dissociable monomers are cohesive when they are neutralized. Gradient polyampholytes exhibit a gradual change in monomer composition from predominantly acidic monomers to predominantly basic monomers. When the nanopore is studied under equilibrium, no applied bias is added, which means  $\Delta V = 0.0 \text{ V}$ . An electrostatic potential difference of  $\Delta V$  between the two reservoirs is applied when ion transport and off-equilibrium properties are studied inside the nanopore. (The convention V = 0 is adopted for the lower reservoir.) (B) Top view and (C) bottom view of the nanopore design. The basic and acidic monomers appear as the main constituents of the polymers at the "entrance" (the lower end) and "exit" (the upper end), respectively.

# **RESULTS AND DISCUSSION**

Morphology Transition and Charge Regulation. It is instructive to first understand the equilibrium structural behavior of the designed nanopore before we investigate its nonequilibrium transport properties upon application of an external field. The brush morphology, the electrostatic potential profile, and the charge distribution within the nanopore are analyzed for three different regimes: (i) lowpH regime, where  $0 \le pH \le 1/2(pK_a^D + pK_a^E) = 7.0$  (D and E represent acidic and basic monomers, respectively); (ii) intermediate-pH regime, where pH = 7.0; and (iii) high-pH regime, where  $7.0 \le pH \le 14.0$ . For each pH regime, one representative pH value is chosen as a test condition, as depicted in Figure 2. At pH = 5.0, a pH lower than both p $K_a^D$ and  $pK_a^E$ , the basic monomers are fully protonated and acquire positive charges, whereas the acidic monomers remain in their neutral state. As shown in Figure 2A and G, the polymers located at the "entrance" (the lower end of the pore) are highly positively charged due to the abundance of basic monomers in that region and, therefore, swollen. In contrast, the polymers at the "exit" (the upper end of the pore) are contracted, as they contain primarily acidic monomers that are neutral at this pH. When pH is switched to 7.0, the polymers adopt the morphology as shown in Figure 2B. At this pH, both weak acidic and basic blocks get partially charged, and the overall electrostatic potential (Figure 2E) and charge distribution (Figure 2H) are "bipolar" as opposed to the "unipolar" ones at

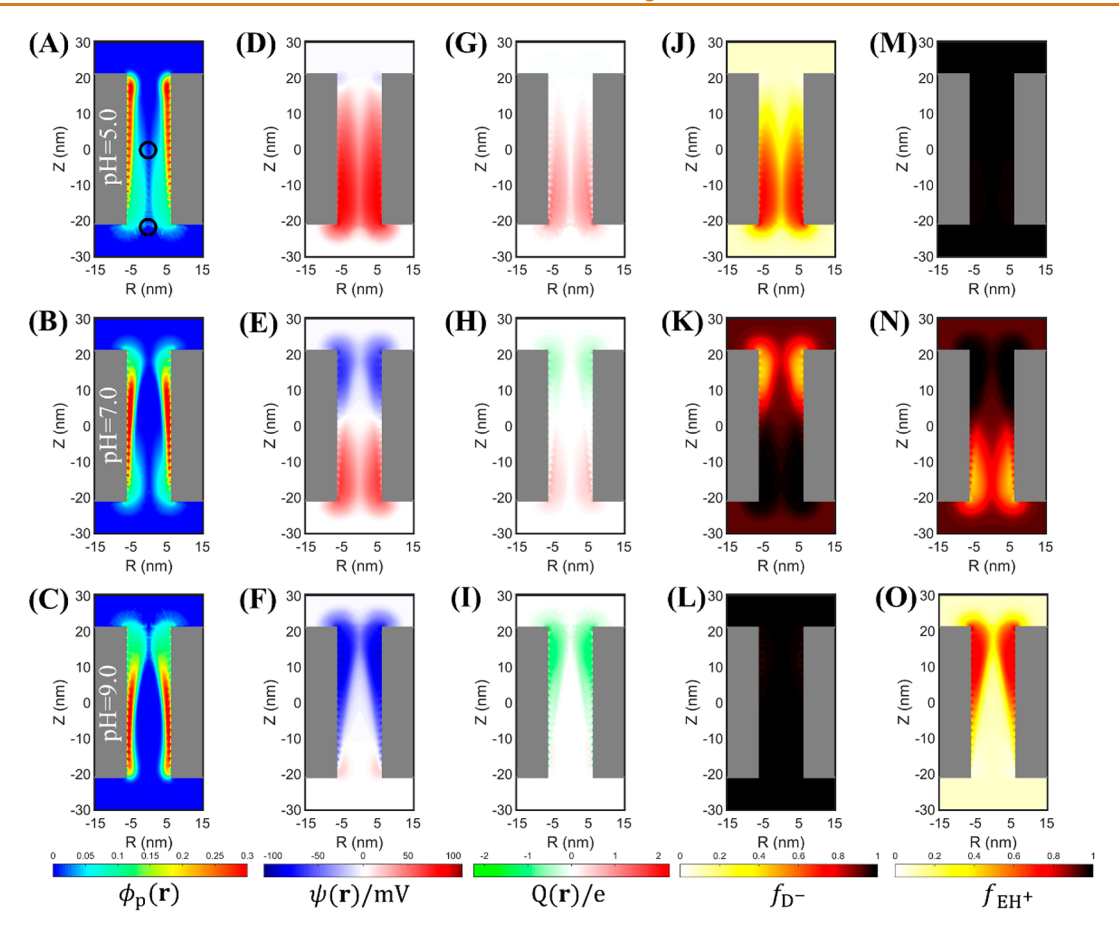


Figure 2. Colormaps of the (A, B, C) polymer volume fraction, (D, E, F) electrostatic potential, (G, H, I) charge distribution under equilibrium, (J, K, L) fraction of charged acidic monomers ( $f_{\rm D}$ ), and (M, N, O) charged basic monomers ( $f_{\rm EH}$ ) at pH = 5.0 (top), 7.0 (middle), and 9.0 (bottom), on a plane containing the pore axis. The black circles in (A) mark the embedded positions of the cargo in the process of passing the nanopore. The weak polyampholytes in the system contain acidic and basic blocks of varying partitions, which leads to asymmetric response to pH changes through the coating. The plots shown here show a variety of asymmetric gating structures, charge environments, and charging behavior, which are all the outcome of the asymmetric pH responsiveness. The chains in the polyampholytemodified pore have a chain length N = 20 and grafting density  $\sigma = 0.245$  nm<sup>-2</sup>. The bulk salt concentration applied here is  $c_{\rm salt} = 0.1$  M.

pH = 5.0 (Figure 2D,G). The electrostatic repulsions among like-charged monomers drive the polymers at both ends to stretch, whereas the intermediate region with intermixed monomers is more contracted. Going to pH = 9.0, the dominant contributor to the polymer charge changes from basic monomers to acidic ones. As a result, the polymers anchored at the upper half domain acquire net negative charges and extend toward the center. Concomitantly, the polymers in another half turn into the uncharged and contracted state. The electrostatic potential becomes "unipolar", again. The asymmetric morphology, electrostatic potential, and charge pattern at pH = 9.0 are shown in Figure 2C,F,I. Although the structural behaviors of the nanopore at pH = 5.0 and pH = 9.0 seem to be reversed, they are not ideally mirrored to each other on closer look. Such subtlety arises because the system does not remain unchanged after exchanging the two different monomers and flipping the nanopore upside down. In the same light, the system is not ideally symmetric at pH = 7.0. More details about the asymmetry inside the brush can be found in the Supporting Information.

The charge fractions at different pH are plotted in Figure 2J-O. Note that the charge fraction can be profoundly different from what is expected in the bulk dilute solution. Such charge regulation happens as a result of the coupling between physical interactions and chemical reaction. When the

pH promotes drastic ionization, the homogeneously charged block will stretch to mitigate strong electrostatic repulsion. Since such stretching is bounded by the contour length of the polymer, the monomers would shift their acid-base equilibria toward neutral state to further lower the electrostatic penalty. Although charge regulation requires chemical work, it is common for end-tethered weak polyelectrolytes. In our design, the polymers have opposingly ionizable blocks and the charge regulation is more complicated than what is expected for weak polyelectrolytes of homotypic ionization. Opposite charge regulation can happen in different blocks. Namely, the majority block tends to have suppressed ionization to lower its intrablock electrostatic repulsion, whereas the minority block has a propensity of augmented ionization to favor its electrostatic attraction with the majority block. Our calculations demonstrate that the nature and degree of charge regulation depend on the local environment of the monomer. In other words, the chemical reaction in the heterogeneous system has local equilibrium, and the charge regulation effect is important for the accurate accounting of ionic conduction in polymer-coated nanopores.

**Current Rectification.** Ion-current rectification is inherent to asymmetric nanopore systems. The above structural analyses suggest that our designed nanopore could serve as an ionic rectifier. Here, we test the rectification performance of

the system by explicitly calculating the ionic conduction (I) under different biased voltages ( $\Delta V$ ). The  $I-\Delta V$  curves at different pH conditions are shown in Figure 3. The asymmetric

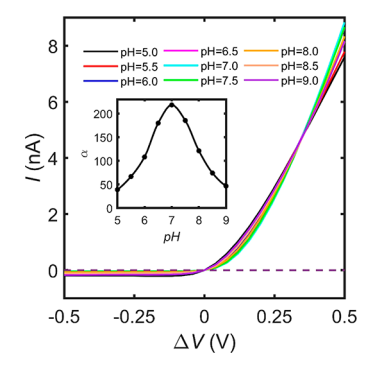


Figure 3. Current–potential curves for the nanopore functionalized with gradient weak polyampholytes. Various curves refer to different pH conditions. Nonohmic responses are observed for all the pH conditions.  $\Delta V < 0$  corresponds to the "OFF" state, while  $\Delta V > 0$  is the "ON" state. The inset in the figure shows the dependency of rectification efficiency  $\alpha$  on the pH conditions. A nonmonotonic behavior happens as a function of pH, with the most efficient rectification found at intermediate pH condition. Calculation parameters: chain length, N=20; grafting density of the polyampholyte chains,  $\sigma=0.245~\mathrm{nm}^{-2}$ ; bulk salt concentration,  $c_{\mathrm{salt}}=0.1~\mathrm{M}$ .

shape of the  $I-\Delta V$  curves indicates that rectification occurs under all test pH conditions. At  $\Delta V < 0$  the system is in a low-conductance (OFF) state, and the high-conductance (ON) state takes place at  $\Delta V > 0$ . To quantify the rectification efficiency, we define a rectification factor  $\alpha = -\frac{I(\Delta V = 0.5 \text{ V})}{I(\Delta V = -0.5 \text{ V})}$ , which is the ratio between the absolute current value in the ON state and the one in the OFF state. The inset of Figure 3 presents the rectification factor as a function of pH. The rectification factor can be higher than 200. Interestingly, the rectification efficiency displays a nonmonotonic trend with a maximum at intermediate pH. To understand the origin of the rectification, we calculate the electrostatic potentials in the presence of different applied biases as shown in Figure 4.

Our calculation reveals the formation of electrostatic traps/ barriers inside the nanopore in the OFF states (Figure 4A), which significantly reduce the mobility of the ionic carriers. In the ON state (Figure 4E), the disappearance of the electrostatic traps/barriers leads to a much higher current. At pH = 5.0 and pH = 9.0, a single trap/barrier is observed, whereas at pH = 7.0 both cation and anion traps/barriers are formed due to the "bipolar" charge pattern inside the nanopore (Figure 4A), which further boosts the rectification factor. To distinguish the contributions of different ions in the ionic conduction, we analyze  $I_{\scriptscriptstyle +}/I_{\rm total}$ , the share that the cation takes from the total current. Figure S4 shows that the major carrier changes from anion at low pH to cation at high pH. On the basis of this ionic selectivity, we can see that it is the trap of major carriers rather than the barrier of the minor carriers that dominates the rectification.

To further optimize the rectification, we systematically study the combinatory effects of pH and salt concentration on ionic conduction. Figure 5 shows the  $I-\Delta V$  curves and rectification factors (see insets of Figure 5) for different pH conditions at varying salt concentrations in the bulk solution. Interestingly, the rectification is not only pH-dependent but also sensitive to

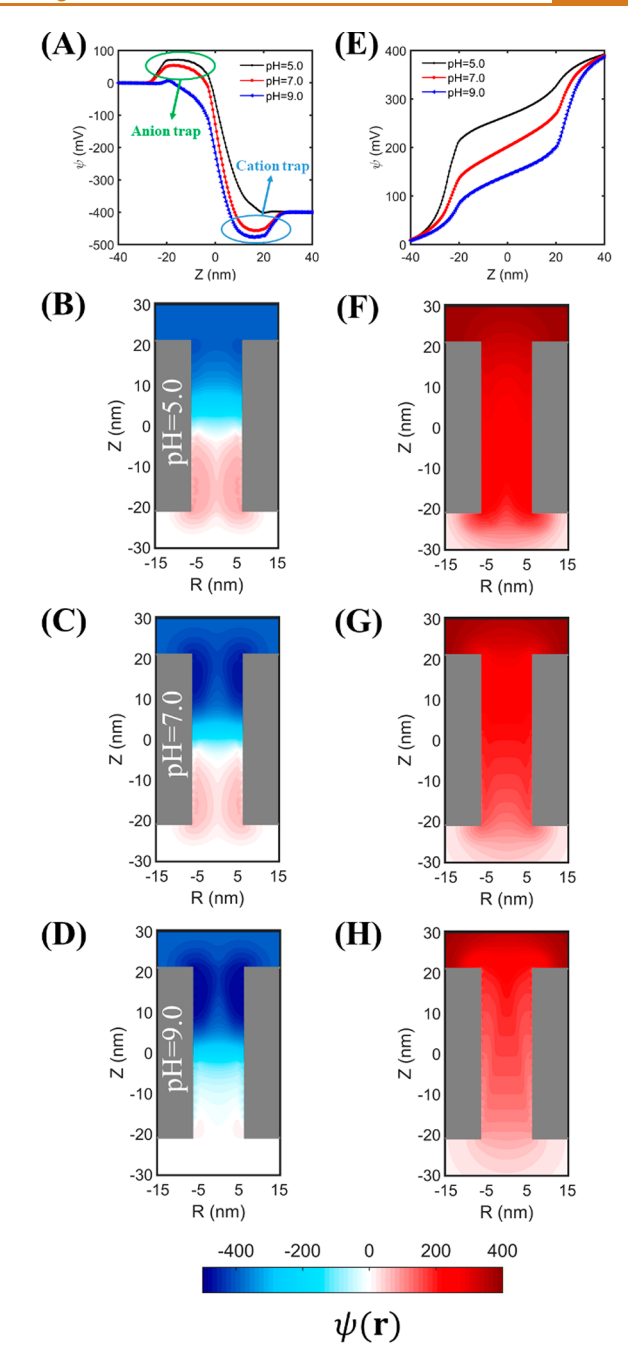


Figure 4. Axial variation of cross-sectional averaged electrostatic potential in the case of (A)  $\Delta V = -0.40$  V and (E)  $\Delta V = 0.40$  V. The plots of electrostatic potential profiles are performed at three representative pH conditions: pH = 5.0, 7.0, and 9.0 respectively. Electrostatic traps for anions and cations are captured in the "OFF" state (traps are marked in A), while the electrostatic traps disappear in the "ON" state (shown in E). Color maps of electrostatic potential in the presence of two characteristic applied potentials, (B, C, D)  $\Delta V = -0.40$  V and (F, G, H)  $\Delta V = 0.40$  V at pH = 5.0 (upper panels), pH = 7.0 (middle panels), and pH = 9.0 (lower panels). Same calculation parameters as in Figure 3.

salt concentration. Although lowering the salt concentration reduces the ionic conduction, it increases the rectification factor. At low salt concentration, the rectification factor can be higher than 1000. To understand how salt concentration influences the rectification, we analyze the electrostatic potentials at different conditions. At the OFF state, we observe

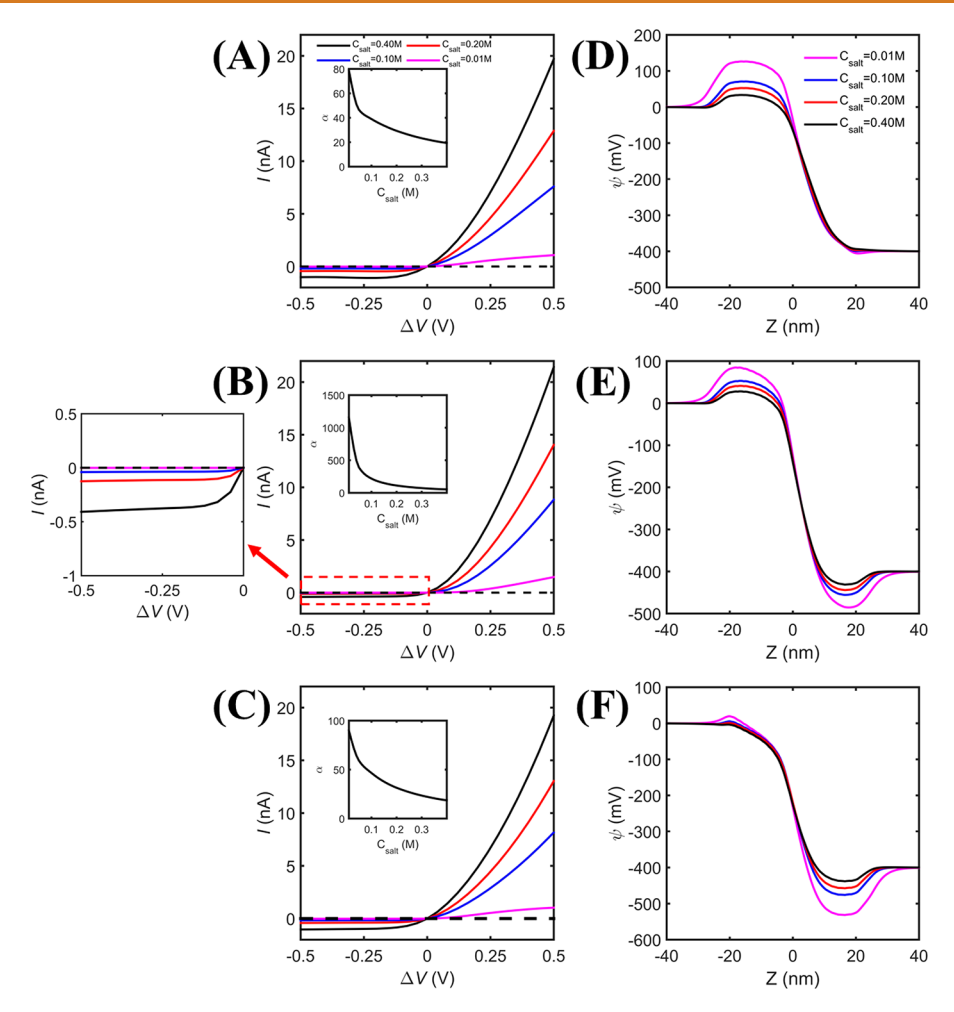


Figure 5. Current-potential curves for the nanopore design in the case of various salt concentrations at (A) pH = 5.0, (B) pH = 7.0, and (C) pH = 9.0. Nonohmic behaviors are observed for all the background salt conditions. The inset shows the dependency of rectification efficiency  $\alpha$  on the salt concentrations. A downtrend in rectification factor happens as the solution gets saltier. Cross-sectional averaged electrostatic potential along the pore axis inside the nanopore functionalized with gradient polyampholytes for different bulk salt concentrations at (D) pH = 5.0, (E) pH = 7.0, and (F) pH = 9.0. The parameters used in the calculations correspond to the same case of Figures 3 and 4, with the exception of salt concentrations.

an enhanced electrostatic trap for the major carriers at lowered salt concentration. This is because the weakened electrostatic screening strengthens the electrostatic attractions between the charged polymers and the major carriers. Importantly, our results reveal a negative correlation between salt concentration and the depth of the electrostatic trap at the OFF state and a positive correlation between this trap depth and the rectification factor. Such correlations indicate that the ionic trapping at the OFF state largely determines the degree of the rectification.

When proposed by Siwy et al. to explain their experimental observation of ionic rectification, 35,36 the ionic trapping model was a qualitative hypothesis that assumes that a linear perturbation of the equilibrium electrostatic potential by an applied biased voltage gives rise to an electrostatic trap for the main current carriers. Our quantitative analysis here can provide numerical evidence for the electrostatic trap in a nanopore. Moreover, our nonequilibrium steady-state theory predicts that the actual ionic traps can be significantly deeper and wider than what are expected under the assumption of linear perturbation (Figure 6). Such a nonlinear electrostatic effect originates from the strong coupling between the polymer morphology, charge regulation, and the ionic transport, which

can be clearly visualized by calculating the difference in the polymer distribution and fraction of charged monomers inside the nanopore with and without an external electric field (Figures S6–S10). It merits a note that capturing such an intricate coupling effect is beyond the capacity of the Poisson–Nernst–Planck (PNP) method,<sup>37–39</sup> which does not consider the conformational change of the coating materials. The nonequilibrium steady-state molecular theory developed here offers a more accurate means to evaluate the ionic rectification of polymer-coated nanopores with high computational efficiency.

Selective Transport of Large Cargoes through the Nanopore. In addition to the smart ionic rectification, the nanopore design can also function as a molecular filter that enables the selective transport of large cargoes, and the selectivity can be adjusted by pH. The potentials of mean forces (PMFs) are calculated for a variety of cargoes to test the selective filtering performance of the nanopore. The PMF at a given position **r** is the work required to bring the cargo from the bulk solution to **r**, which can be expressed as follows:

$$\Delta F_{\text{pmf}} = F(\mathbf{r}_{\text{cargo}} = \mathbf{r}) - F(\mathbf{r}_{\text{cargo}} = \mathbf{r}_{\text{ref}})$$
(1)

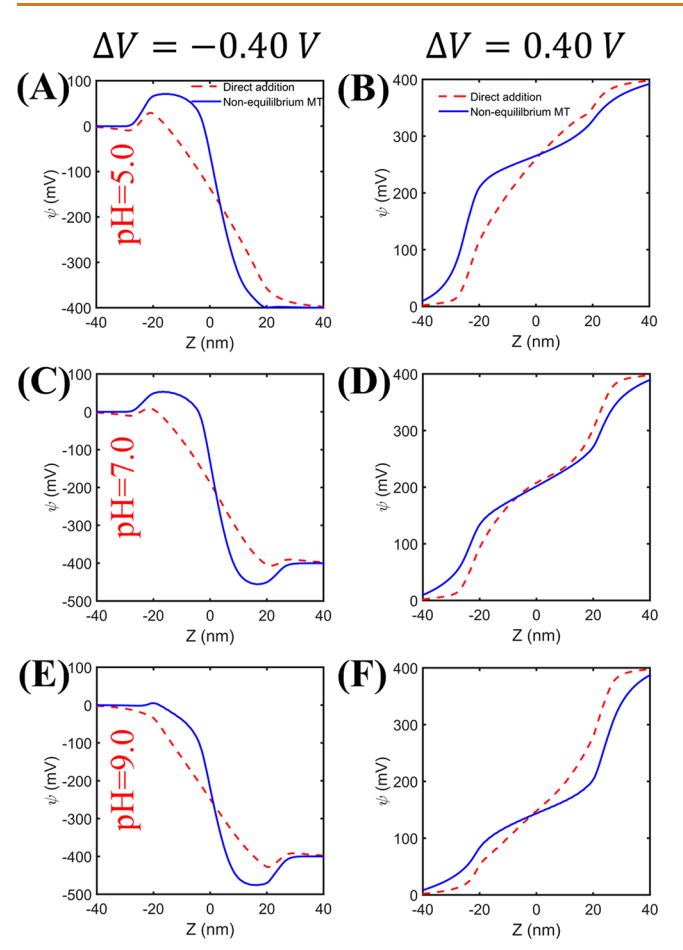


Figure 6. Cross-sectional averaged electrostatic potential along the axis of a nanopore when  $\Delta V = -0.40~\rm V$  (left) and  $\Delta V = 0.40~\rm V$  (right). The dashed red lines show the outcome of linear superposition of equilibrium electrostatic potential and the applied biased potential that drives the system out of equilibrium, whereas the blue solid lines show the calculations of the nonequilibrium steady-state molecular theory. The differences between these two plots exhibit the strong nonlinear coupling between these two potentials.

The cargo located in the bulk solution is selected as the reference system, where the free energy is set to be zero. There are three different cargos studied here, namely, positively charged, neutral, and negatively charged. These cargoes are all considered to be hydrophilic. The cargoes are 1.5 nm in radius, and the charge amplitude of the charged cargoes is chosen to be 4.5e. The nanopores modified by grafting polymers at surface coverage  $\sigma = 0.245$  nm<sup>-2</sup> and  $\sigma = 0.1225$  nm<sup>-2</sup> are both used for the transport test of cargo transport. The PMF test is also performed in a wide window of pH conditions to further check the dependence of the selectivity on pH.

We present in Figure 7A, B, and C the PMFs as a function of the distance from the particle center to the nanopore axial center for these three types of translocating cargos. The corresponding grafting density of the tethered polymer chains in this case is  $\sigma = 0.245~\rm nm^{-2}$ . A cargo experiencing an energy barrier much larger than the thermal fluctuation will be blocked by the pore. In Figure 7A, a huge potential barrier located near the entrance is observed for the positively charged cargo at relatively low pH values. In that pH range, the polymers at the entrance have a net positive charge and adopt a stretched conformation. Hence, the polymers repel the

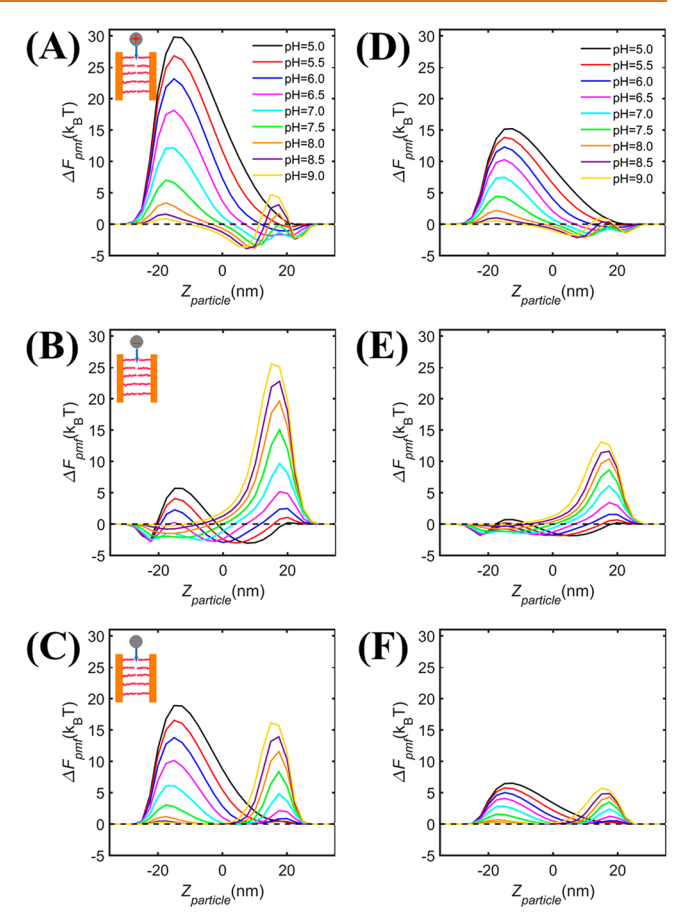


Figure 7. Potential of mean forces (PMFs) of the transport of (A, D) positively, (B, E) negatively, and (C, F) neutrally charged cargo. Various curves correspond to the transport behavior of the cargo under different pH conditions. The grafting density of the polyampholyte chains tethered in the nanopore equals  $\sigma_g=0.245$  nm $^{-2}$  (left panels) and  $\sigma_g=0.1225$  nm $^{-2}$  (right panels), respectively. Inset: Scheme of the translocation of the cargo through the nanopore along the center axis.

positive cargo with both electrostatic repulsion and steric hindrance. A drop in the barrier happens along with the increasing pH due to a decrease in fraction of charged basic monomers  $(f_{\mathrm{EH}^+})$  and contraction of polymers, which gradually weakens the repulsions. The increase of pH can also induce the deprotonation of the acidic monomers concentrated at the exit. Consequently, the polymers near the exit, carrying net negative charges, protrude toward the center to repel the positive cargo. However, only a low free energy barrier is formed because the steric repulsions and the electrostatic attractions balance each other. This trend implies that cargos carrying positive charges are selected to translocate through the nanopore with less resistance at relatively high pHs. Note that two energy wells observed at high pHs correspond to the state of positive cargos embedding in the polymer brush without penetrating it. The absence of polymers can be clearly detected at the embedded position marked in Figure 2A, indicating a low overlap between the cargo and the polymers. Therefore, the long-range electrostatic attraction overcomes the steric repulsion at this position, which give rises to the energy well. Figure 7B shows the PMFs of negatively charged cargoes translocating through the nanopore. It is not surprising that the overall profiles of the PMFs look reversed to those of the positively charged cargoes, since the two ends of the nanopore undergo different ionizations. However, such reversal is not ideal because the upper and lower parts of the pore do not perfectly mirror each other. Our results demonstrate that the cargo is able to probe subtle environmental changes in the nanopore.

Figure 7C compares the transport behavior of the neutral cargo under different pH conditions. At low pHs, the stretched polymers at the entrance repel the neutral cargo with pure steric repulsion, which is the origin of the barrier in this area. The absence of electrostatic repulsion leads to a lower energy barrier compared to the one observed at the same position for positive cargo. At high pH values, the swelling conformation of the polymers at the other side results in the emergence of the energy barrier at the exit, whereas the barrier at the entrance starts to fade away due to the contraction of polymers there. At intermediary pH, polymers at both ends are in a slightly swollen state (see Figure 2B), and thus the coexistence of the two barriers ensues. However, the maximum height of these two barriers is reduced, which promotes the passage of the cargo through the nanopore.

The above characterizations have shown that the selective transport of large cargoes through the nanopore can be easily tuned by pH. To have a more systematic understanding of such selective permeability, we repeated our calculations for a lower grafting density of the polymer brush. Figure 7D, E, and F demonstrate that the qualitative pH dependence of the PMFs is preserved in this sparser case of coating. However, the overall free energy landscape is flattened, which weakens the energy barriers for the blocked cargoes but allows a more efficient transport for the selected cargoes. This trend implies that a proper choice of the grafting density can optimize the pH-tunable cargo selectivity.

Ion Pumping. In this proposed nanopore, the polymers anchored at the two sides have opposite pH-responsiveness due to their different main constituent blocks. The changes in the morphologies and ionization states of the polymers are then driven by pH changes to alternately form open and closed gating states at the two sides, which has the potential of serving as an ion pump. On the basis of the cooperate pH-responsive double gates, we demonstrate in Figure 8 the whole process of ion pumping under the condition that the anion/cation concentration is higher/lower in the upper reservoir compared with the lower one. It should be mentioned that the applied voltage, 0.50 V (ON state), serves as the external energy source to drive the ions in and out of the nanopore in our system. At pH = 5.0 (see Figure 8A), the positively charged polymers at the lower end of the pore function as an open gate. It allows anions to enter the nanopore from the lower reservoir and cations to be released into the lower reservoir. The polymers at the other end are nearly neutral, corresponding to the closed state. The ion transport is therefore blocked at the upper end of the pore.

Then by switching the pH to 9.0 (see Figure 8B), the negative-charge-containing upper end changes from the closed state to the open state, and the other end stops the ion transport. In this case, cations are attracted into the nanopore from the upper reservoir, while the anions are repelled to the lower one. Hence, by alternating between these two pH conditions, ions are forced to move against their concentration gradient and a cycle of ion pumping can be accomplished. A bioinspired ion pump based on two homopolymer gates has already been realized experimentally by Zhang *et al.*<sup>40</sup> Our prior work shows that diblock copolymer coating can optimize

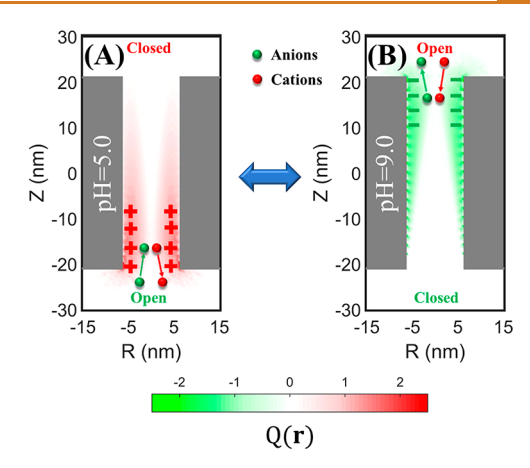


Figure 8. Color maps of the charge distribution on a plane normal to the pore axis at (A) pH = 5.0 and (B) pH = 9.0 in the presence of the applied bias  $\Delta V = 0.50~\rm V$  ("ON" state). The corresponding schematic representations of the ion pumping process resulting from respectively stimulating the polyampholytes at the two sides by manually continuous pH stimuli switching between pH = 5.0 and pH = 9.0 at 0.50 V.

the structure of the double gates.<sup>23</sup> The design in this work further demonstrates that continuous copolymer grafting with compositional gradient can serve as an alternative way to enable ionic pumping.

It is known that the nanopore entrance is prone to concentration polarization, a phenomenon that limits the forward current as it promotes backward ionic diffusion. One advantage of our coating design is that the asymmetric charge distribution of the polymer brush can prevent strong concentration polarization. To demonstrate this property, we analyzed the concentration profiles of the majority carriers at pH = 5.0 and 9.0 along the pore axis and verified that the depletion layers are missing at both pH conditions (Figure S12).

### **CONCLUSIONS**

In the present work, we proposed an asymmetric nanopore design in which the symmetry of the system is broken by coating the inner wall of the pore with an asymmetric weak polyampholyte brush whose main component changes gradually from acidic to basic along the axis of the pore. We used both equilibrium and nonequilibrium molecular theories to systematically study the molecular organizations and transport properties of the designed nanopore. By explicitly considering the polymer conformations, the coupling between physical interactions and chemical reaction, our model is able to capture the shift of acid-base equilibrium under nanoconfinement and the polymer deformation under the biased voltage. Our calculations reveal that the asymmetric polymer coating under different pH exhibits a wealth of asymmetric morphologies and charge patterns. In general, the polyampholyte brush creates a unipolar electrostatic environment at low and high pHs, versus the bipolar electrostatic environment at intermediate pHs. We further predict that these polar environments lead to electrostatic traps for the major carriers of ionic currents through the pore for one polarity of the external voltage. In particular, the unipolar environment results in a single trap, whereas double traps appear in the bipolar environment. By characterizing the ionic conductivity as a function of the applied biased voltage, we demonstrate that the

designed nanopore can serve as an ionic rectifier whose rectification factor can be controlled by pH and salt concentration. When strong double traps are formed at intermediate pH and low salt concentration, the rectification factor can go above 1000. Our study highlights ionic trapping as an important rectifying mechanism inside nanopores and offers quantitative insights into the relation between the trap depth and the rectification efficiency. Moreover, our study shows a strong nonlinear effect of the applied biased voltage on the electrostatic potential inside the nanopore. Namely, the external electrostatic field and the intrinsic electrostatic potential at equilibrium are nonadditive.

Beyond ionic rectification, our designed nanopore can also function as a molecular filter for large cargoes. The free energy landscape of the cargo translocating through the nanopore is largely determined by the steric and electrostatic interactions between the cargo and the polymers and is sensitive to the pH. Since the coating component is varying along the axis of the pore, the PMF of the cargo is asymmetric, with the major barrier position and height being pH-dependent. Such a pH response of the barrier allows the nanopore to serve as an ionic pump with alternating open and closed polymer states at its two ends.

In summary, our theoretical results demonstrate that the asymmetric polymer anchorage and sequence design successfully translate into structural assemblies and eventually into functional gates for different types of cargoes. We hope these theoretical insights can inspire and guide experimental efforts on building smart nanopores with asymmetric functionalization.

### **METHODS**

In order to have a comprehensive understanding of the properties of the proposed nanopore and to explore its potential functions, it is necessary to study the structural and thermodynamic behaviors of the functionalized polymer coating under both equilibrium and nonequilibrium conditions. Equilibrium molecular theory has been proven to be successful in predicting the structure of the end-tethered polymers in nanopores or nanochannels.<sup>23,41-43</sup> On the basis of this theoretical framework, a nonequilibrium version of molecular theory was derived by considering the generalized diffusion equation of the ions in the system. 44,45 The nonequilibrium steady-state theory is a powerful tool in studying the off-equilibrium molecular organization of the system and its transport properties. However, that nonequilibrium molecular theoretical approach still had its restrictions. In particular, acid-base equilibrium has not been taken into account, which limits our studies to molecular transport through the nanopores functionalized with strong polyelectrolytes. In the present work, we extend our model to address the complex charge regulation process under nanoconfinement. The theory will be outlined in this section and detailed in the Supporting Information.

**Equilibrium Molecular Theory.** The previously developed equilibrium molecular theory  $^{23,46-49}$  explicitly considers the shape, charge, size, and conformations of all molecular species in the system. Moreover, it incorporates the relevant intra- and intermolecular interactions such as long-range electrostatic interactions, steric repulsions, and van der Waals (vdW) forces. For weak polyelectrolytes, the presence of the acid—base equilibrium is taken into consideration. The basic idea of the theory is to solve the free energy functional of the system in a self-consistent way. A large set of polymer conformations are input into the theory, and the minimization of free energy determines the probability of finding the polymer in certain conformation  $\alpha$ ,  $P(\mathbf{r}, \alpha)$ , as well as the equilibrium distribution of all molecular species. Polymer conformations are generated using the rotational isometric state model (RIS) and are rejected if not self-avoiding or if overlapped with the walls of

the nanopore. The theory has been shown to be in excellent agreement with, for example, computer simulations  $^{50}$  as well as experimental observations  $^{41,46,51,52}$  for structural and thermodynamic properties of polymer-grafted systems.

We minimize the free energy of the system, which has the following general contributions:

$$F = -TS_{\text{poly}} - TS_{\text{mix}} + E_{\text{vdW}} + E_{\text{electro}} + F_{\text{acid-base}}^{\text{mix}} + E_{\text{cargo}}$$
(2)

The first term  $-TS_{poly}$  in eq 2 is the contribution arising from the conformational entropy of the polymer. More specifically, the conformational entropy is given by  $\sum_{\alpha} P(\alpha)$  In $P(\alpha)$ . The second term describes the mixing (or translational) entropy of the solvent (water), cations, anions, protons, and hydroxyl ions. The third term represents the van der Waals effective attractive energy between polymer beads. The fourth term denotes the electrostatic contribution to the free energy of the system. The subsequent contribution to the free energy functional accounts for the energetic and entropic contributions stemming from the chemical acid-base equilibrium. The last term in eq 2 stands for the steric and electrostatic interactions between the particle and the polymers. For more information on a detailed description of the theoretical framework, molecular model, and minimization of the free energy, please refer to the Supporting Information. It is necessary to stress that to increase the computation efficiency, we take advantage of the cylindrical symmetry of the system and assume azimuthal homogeneity, meaning that all the position-related quantities vary only in the radial and axial

Nonequilibrium Steady-State Molecular Theory. In addition to the equilibrium properties of the nanopore system, we also investigate the ion transport behavior inside the pore with the state-of-the-art nonequilibrium steady-state molecular theory. Our theoretical framework combines a previously developed nonequilibrium molecular theory 44,45 with a consideration of acid—base equilibrium. In this approach, we take the local equilibrium approximation and make the chemical potential a spatial variable. This approximation states that the thermodynamic variables in the system can be defined locally and the equilibrium functional relationships among them in a nonequilibrium system are still valid. In our case, the mass fluxes are driven by the chemical potential gradients that arise due to the applied bias. Within the linear response regime, the fluxes of ions can be written as

$$\mathbf{J}_{i}(\mathbf{r},t) = -D_{i}\rho_{i}(\mathbf{r},t)\nabla\beta\mu_{i}(\mathbf{r},t)$$
(3)

where i = A, C,  $H^+$ , and  $OH^-$ , and  $D_i$  is the diffusion coefficient for different ions.  $\rho_i(\mathbf{r},t)$  and  $\mu_i(\mathbf{r},t)$  represent the density and chemical potential of the species i at position  $\mathbf{r}$  and time t, respectively. At this point, we introduce the steady-state condition. As a consequence of this approximation, all variables are considered to be time-independent hereafter. At steady state, the relationship between the density of mobile ions and mass flux can be expressed as

$$\frac{\partial \rho_i(\mathbf{r})}{\partial t} = -\nabla \mathbf{J}_i(\mathbf{r}) = \nabla [D_i \rho_i(\mathbf{r}, t) \nabla \beta \mu_i(\mathbf{r}, t)] = 0$$
(4)

Our approach to obtain the chemical potential in eq 4 is to first write down an explicit expression for the semi-grand canonical potential of the system, which can be found in eq S40 in the Supporting Information. The minimization of the functional with respect to  $\rho_i(\mathbf{r})$  yields the detailed formulation of  $\mu_i(\mathbf{r})$ :

$$\beta \mu_i(\mathbf{r}) = \text{In}(\rho_i(\mathbf{r})\nu_w) + \nu_i \beta \pi(\mathbf{r}) + q_i \beta \psi(\mathbf{r})$$
(5)

where  $q_i$  is the charge of the species *i*. Then the explicit formulation of mass flux can be obtained by substituting eq 5 into eq 3:

$$\mathbf{J}_{i}(\mathbf{r}) = -D_{i}\nabla\rho_{i}(\mathbf{r}) - D_{i}\rho_{i}(\mathbf{r})q_{i}\nabla\beta\psi(\mathbf{r}) - D_{i}\rho_{i}(\mathbf{r})\nu_{i}\nabla\beta\pi(\mathbf{r})$$
(6)

It is noteworthy that the mass fluxes of mobile ion species shown in eq 6 are driven by the gradient of ion concentration, the gradient of electrostatic potential, and the gradient of the osmotic pressure. The

explicit expressions for the system parameters  $(\rho_i(\mathbf{r}), P(\mathbf{r}, \alpha), f_i(\mathbf{r}))$ can still be obtained through minimization of the free energy functional. The detailed formulations are listed in eq S51 to eq S62 in the Supporting Information. The unknowns that need to be determined are the lateral pressures  $\pi(\mathbf{r})$ , the electrostatic potentials  $\psi(\mathbf{r})$ , and the number densities of mobile ions. The solutions can be obtained in the following ways. The detailed expressions for the variables that define the structure of the system, including ion fluxes, are substituted into the continuity equation mentioned above, together with incompressibility constraint and the Poisson equation, resulting in a set of integro-differential equations, whose solutions determine all those unknowns. This problem lacks an analytical solution, and thus we discretize the space to convert the differential equations into a system of coupled nonlinear equations, which we can then solve self-consistently<sup>44</sup> for those unknowns. Details concerning the discretization and numerical methodology can be found in our previous publications.44

Polymer Sequence Design and System Details. The nanopore studied in the present work is shown in Figure 1. The dimensions of the nanopore are 13 nm in diameter and 42 nm in length. The reservoirs contain salt anions and cations, as well as protons (H+) and hydroxyl ions (OH-). The inner wall of the nanopore is modified by grafting polyampholytes, and each chain contains 20 segments. The monomers that construct the bottom component are acidic (termed as D) and the  $pK_a^D$  is set to be 6. The top block carries basic monomers (termed as E) with  $pK_a^E$  set to be 8. Both kinds of ionizable monomers are cohesive when they are neutralized. The interaction parameters between the same species are  $\varepsilon_{\rm D,\;D}=\varepsilon_{\rm E,\;E}=1.0k_{\rm B}T$  and the cross-species  $\varepsilon_{\rm D,\;E}=1.0k_{\rm B}T$ . There are 21 grafting heights on the inner surface of the nanopore, with a spacing of 2 nm in-between. Twenty copies of polymers are tethered at each height, rendering a surface coverage density  $\sigma = 0.245 \text{ nm}^{-2}$ . Unless specifically mentioned hereafter, the grafting density is maintained at this value. The polymers anchored at different grafting position vary in sequence. These sequences are denoted by  $D_x E_y$ . The polymers exhibit a gradient change in composition from predominantly basic monomer to mostly acidic monomer. In particular, the length of acidic block increases from 0 (x = 0) at the "entrance" (the lower end of the pore) to 20 (x = 20) at the "exit" (the upper end), while the opposite trend happens for a basic block. A potential difference  $\Delta V$  is applied between reversible electrodes located in each reservoir when the ionic transport properties of the pore are studied. The lower reservoir is grounded (V = 0) conventionally.

For simplicity and to better focus on understanding the molecular mechanisms underlying the nanopore functions, we limit our study to a system of fixed parameters, such as pore dimension, polymer grafting density, and compositional gradient, that are chosen based on our knowledge from prior works. <sup>23,42,45</sup> It is expected that the performance of our system can be further optimized by tuning the system parameters. However, we believe that a difference choice of parameters will not change the qualitative conclusions made in our current work. The effects of the system parameters will be covered more systematically in our future studies.

# **ASSOCIATED CONTENT**

# **5** Supporting Information

The Supporting Information is available free of charge at https://pubs.acs.org/doi/10.1021/acsnano.1c05543.

Detailed description of the theoretical methods and molecular model; additional analysis of the asymmetry in morphology and charging behavior; supporting data of the reorganization of polyelectrolytes in the presence of large applied bias (PDF)

### **AUTHOR INFORMATION**

### **Corresponding Authors**

Kai Huang – Institute of Systems and Physical Biology, Shenzhen Bay Laboratory, Shenzhen 518107, China; Email: huangkai@szbl.ac.cn

Igal Szleifer — Department of Biomedical Engineering,
Department of Chemistry, and Chemistry of Life Processes
Institute, Northwestern University, Evanston, Illinois 60208,
United States; orcid.org/0000-0002-8708-0335;
Email: igalsz@northwestern.edu

### **Author**

Shiyi Qin — Department of Biomedical Engineering,
Department of Chemistry, and Chemistry of Life Processes
Institute, Northwestern University, Evanston, Illinois 60208,
United States; orcid.org/0000-0002-8811-914X

Complete contact information is available at: https://pubs.acs.org/10.1021/acsnano.1c05543

### **Notes**

The authors declare no competing financial interest.

### **ACKNOWLEDGMENTS**

I.S. acknowledges support from the National Science Foundation under Grant CBET-1833214. K.H. acknowledges support from the Shenzhen Bay Laboratory.

### **REFERENCES**

- (1) Siwy, Z.; Trofin, L.; Kohli, P.; Baker, L. A.; Trautmann, C.; Martin, C. R. Protein Biosensors Based on Biofunctionalized Conical Gold Nanotubes. *J. Am. Chem. Soc.* **2005**, *127* (14), 5000–5001.
- (2) Martin, C. R.; Siwy, Z. S. CHEMISTRY: Learning Nature's Way: Biosensing with Synthetic Nanopores. *Science (Washington, DC, U. S.)* **2007**, 317 (5836), 331–332.
- (3) Ali, M.; Yameen, B.; Neumann, R.; Ensinger, W.; Knoll, W.; Azzaroni, O. Biosensing and Supramolecular Bioconjugation in Single Conical Polymer Nanochannels. Facile Incorporation of Biorecognition Elements into Nanoconfined Geometries. *J. Am. Chem. Soc.* **2008**, 130 (48), 16351–16357.
- (4) de la Escosura-Muñiz, A.; Merkoçi, A. Nanochannels Preparation and Application in Biosensing. ACS Nano 2012, 6 (9), 7556–7583.
- (5) Wang, J.; Hou, J.; Zhang, H.; Tian, Y.; Jiang, L. Single Nanochannel-Aptamer-Based Biosensor for Ultrasensitive and Selective Cocaine Detection. ACS Appl. Mater. Interfaces 2018, 10 (2), 2033–2039.
- (6) Cai, X.; Cao, S.; Cai, S.; Wu, Y.; Ajmal, M.; Li, Y. Reversing Current Rectification to Improve DNA-Sensing Sensitivity in Conical Nanopores. *Electrophoresis* **2019**, 40 (16–17), 2098–2103.
- (7) Xie, Y.; Wang, X.; Xue, J.; Jin, K.; Chen, L.; Wang, Y. Electric Energy Generation in Single Track-Etched Nanopores. *Appl. Phys. Lett.* **2008**, 93 (16), 163116.
- (8) Siria, A.; Poncharal, P.; Biance, A.-L.; Fulcrand, R.; Blase, X.; Purcell, S. T.; Bocquet, L. Giant Osmotic Energy Conversion Measured in a Single Transmembrane Boron Nitride Nanotube. *Nature* **2013**, 494 (7438), 455–458.
- (9) Ma, T.; Balanzat, E.; Janot, J.-M.; Balme, S. Nanopore Functionalized by Highly Charged Hydrogels for Osmotic Energy Harvesting. ACS Appl. Mater. Interfaces 2019, 11 (13), 12578–12585.
- (10) Macha, M.; Marion, S.; Nandigana, V. V. R.; Radenovic, A. 2D Materials as an Emerging Platform for Nanopore-Based Power Generation. *Nat. Rev. Mater.* **2019**, *4* (9), 588–605.
- (11) Adiga, S. P.; Brenner, D. W. Flow Control through Polymer-Grafted Smart Nanofluidic Channels: Molecular Dynamics Simulations. *Nano Lett.* **2005**, *5* (12), 2509–2514.

- (12) He, Z.; Zhou, J.; Lu, X.; Corry, B. Bioinspired Graphene Nanopores with Voltage-Tunable Ion Selectivity for Na+ and K+. ACS Nano 2013, 7 (11), 10148–10157.
- (13) Lam, M. H.; Briggs, K.; Kastritis, K.; Magill, M.; Madejski, G. R.; McGrath, J. L.; de Haan, H. W.; Tabard-Cossa, V. Entropic Trapping of DNA with a Nanofiltered Nanopore. *ACS Appl. Nano Mater.* **2019**, 2 (8), 4773–4781.
- (14) Hou, X.; Guo, W.; Jiang, L. Biomimetic Smart Nanopores and Nanochannels. *Chem. Soc. Rev.* **2011**, 40 (5), 2385.
- (15) Kowalczyk, S. W.; Blosser, T. R.; Dekker, C. Biomimetic Nanopores: Learning from and about Nature. *Trends Biotechnol.* **2011**, 29 (12), 607–614.
- (16) Kowalczyk, S. W.; Kapinos, L.; Blosser, T. R.; Magalhães, T.; van Nies, P.; Lim, R. Y. H.; Dekker, C. Single-Molecule Transport across an Individual Biomimetic Nuclear Pore Complex. *Nat. Nanotechnol.* **2011**, *6* (7), 433–438.
- (17) Jovanovic-Talisman, T.; Tetenbaum-Novatt, J.; McKenney, A. S.; Zilman, A.; Peters, R.; Rout, M. P.; Chait, B. T. Artificial Nanopores That Mimic the Transport Selectivity of the Nuclear Pore Complex. *Nature* **2009**, *457* (7232), 1023–1027.
- (18) Lanphere, C.; Arnott, P. M.; Jones, S. F.; Korlova, K.; Howorka, S. A Biomimetic DNA-Based Membrane Gate for Protein-Controlled Transport of Cytotoxic Drugs. *Angew. Chem.* **2021**, *133* (4), 1931–1936.
- (19) de Groot, G. W.; Santonicola, M. G.; Sugihara, K.; Zambelli, T.; Reimhult, E.; Vörös, J.; Vancso, G. J. Switching Transport through Nanopores with PH-Responsive Polymer Brushes for Controlled Ion Permeability. *ACS Appl. Mater. Interfaces* **2013**, 5 (4), 1400–1407.
- (20) Yusko, E. C.; Johnson, J. M.; Majd, S.; Prangkio, P.; Rollings, R. C.; Li, J.; Yang, J.; Mayer, M. Controlling Protein Translocation through Nanopores with Bio-Inspired Fluid Walls. *Nat. Nanotechnol.* **2011**, *6* (4), 253–260.
- (21) Wanunu, M.; Meller, A. Chemically Modified Solid-State Nanopores. *Nano Lett.* **2007**, *7* (6), 1580–1585.
- (22) Li, C.-Y.; Ma, F.-X.; Wu, Z.-Q.; Gao, H.-L.; Shao, W.-T.; Wang, K.; Xia, X.-H. Solution-PH-Modulated Rectification of Ionic Current in Highly Ordered Nanochannel Arrays Patterned with Chemical Functional Groups at Designed Positions. *Adv. Funct. Mater.* **2013**, 23 (31), 3836–3844.
- (23) Huang, K.; Szleifer, I. Design of Multifunctional Nanogate in Response to Multiple External Stimuli Using Amphiphilic Diblock Copolymer. *J. Am. Chem. Soc.* **2017**, *139* (18), 6422–6430.
- (24) Yameen, B.; Ali, M.; Neumann, R.; Ensinger, W.; Knoll, W.; Azzaroni, O. Ionic Transport through Single Solid-State Nanopores Controlled with Thermally Nanoactuated Macromolecular Gates. *Small* **2009**, *5* (11), 1287–1291.
- (25) Guo, W.; Xia, H.; Xia, F.; Hou, X.; Cao, L.; Wang, L.; Xue, J.; Zhang, G.; Song, Y.; Zhu, D.; Wang, Y.; Jiang, L. Current Rectification in Temperature-Responsive Single Nanopores. *ChemPhysChem* **2010**, *11* (4), 859–864.
- (26) Cheng, L.; Cao, D. Designing a Thermo-Switchable Channel for Nanofluidic Controllable Transportation. *ACS Nano* **2011**, *5* (2), 1102–1108.
- (27) Zhou, Y.; Guo, W.; Cheng, J.; Liu, Y.; Li, J.; Jiang, L. High-Temperature Gating of Solid-State Nanopores with Thermo-Responsive Macromolecular Nanoactuators in Ionic Liquids. *Adv. Mater.* **2012**, 24 (7), 962–967.
- (28) Liu; Dunphy, D. R.; Atanassov, P.; Bunge, S. D.; Chen, Z.; López, G. P.; Boyle, T. J.; Brinker, C. J. Photoregulation of Mass Transport through a Photoresponsive Azobenzene-Modified Nanoporous Membrane. *Nano Lett.* **2004**, *4* (4), 551–554.
- (29) Wang, G.; Bohaty, A. K.; Zharov, I.; White, H. S. Photon Gated Transport at the Glass Nanopore Electrode. *J. Am. Chem. Soc.* **2006**, 128 (41), 13553–13558.
- (30) Rao, S.; Lu, S.; Guo, Z.; Li, Y.; Chen, D.; Xiang, Y. A Light-Powered Bio-Capacitor with Nanochannel Modulation. *Adv. Mater.* **2014**, *26* (33), 5846–5850.

- (31) Jiang, Y.; Lee, A.; Chen, J.; Ruta, V.; Cadene, M.; Chait, B. T.; MacKinnon, R. X-Ray Structure of a Voltage-Dependent K+ Channel. *Nature* **2003**, *423* (6935), 33–41.
- (32) Harrell, C. C.; Kohli, P.; Siwy, Z.; Martin, C. R. DNA–Nanotube Artificial Ion Channels. *J. Am. Chem. Soc.* **2004**, *126* (48), 15646–15647.
- (33) Perez Sirkin, Y. A.; Szleifer, I.; Tagliazucchi, M. Voltage-Triggered Structural Switching of Polyelectrolyte-Modified Nanochannels. *Macromolecules* **2020**, *53* (7), 2616–2626.
- (34) Huang, K.; Tagliazucchi, M.; Park, S. H.; Rabin, Y.; Szleifer, I. Nanocompartmentalization of the Nuclear Pore Lumen. *Biophys. J.* **2020**, *118* (1), 219–231.
- (35) Siwy, Z.; Heins, E.; Harrell, C. C.; Kohli, P.; Martin, C. R. Conical-Nanotube Ion-Current Rectifiers: The Role of Surface Charge. *J. Am. Chem. Soc.* **2004**, *126* (35), 10850–10851.
- (36) Siwy, Z. S. Ion-Current Rectification in Nanopores and Nanotubes with Broken Symmetry. *Adv. Funct. Mater.* **2006**, *16* (6), 735–746.
- (37) Zeng, Z.; Ai, Y.; Qian, S. PH-Regulated Ionic Current Rectification in Conical Nanopores Functionalized with Polyelectrolyte Brushes. *Phys. Chem. Chem. Phys.* **2014**, *16* (6), 2465–2474.
- (38) Hsu, J.-P.; Wu, H.-H.; Lin, C.-Y.; Tseng, S. Importance of Polyelectrolyte Modification for Rectifying the Ionic Current in Conically Shaped Nanochannels. *Phys. Chem. Chem. Phys.* **2017**, 19 (7), 5351–5360.
- (39) Jiang, Y.; Feng, Y.; Su, J.; Nie, J.; Cao, L.; Mao, L.; Jiang, L.; Guo, W. On the Origin of Ionic Rectification in DNA-Stuffed Nanopores: The Breaking and Retrieving Symmetry. *J. Am. Chem. Soc.* **2017**, *139* (51), 18739–18746.
- (40) Zhang, H.; Hou, X.; Zeng, L.; Yang, F.; Li, L.; Yan, D.; Tian, Y.; Jiang, L. Bioinspired Artificial Single Ion Pump. *J. Am. Chem. Soc.* **2013**, *135* (43), 16102–16110.
- (41) Tagliazucchi, M.; Azzaroni, O.; Szleifer, I. Responsive Polymers End-Tethered in Solid-State Nanochannels: When Nanoconfinement Really Matters. *J. Am. Chem. Soc.* **2010**, *132* (35), 12404–12411.
- (42) Peleg, O.; Tagliazucchi, M.; Kröger, M.; Rabin, Y.; Szleifer, I. Morphology Control of Hairy Nanopores. *ACS Nano* **2011**, *5* (6), 4737–4747.
- (43) Tagliazucchi, M.; Szleifer, I. How Does Confinement Change Ligand—Receptor Binding Equilibrium? Protein Binding in Nanopores and Nanochannels. *J. Am. Chem. Soc.* **2015**, *137* (39), 12539—12551.
- (44) Tagliazucchi, M.; Rabin, Y.; Szleifer, I. Ion Transport and Molecular Organization Are Coupled in Polyelectrolyte-Modified Nanopores. *J. Am. Chem. Soc.* **2011**, *133* (44), 17753–17763.
- (45) Tagliazucchi, M.; Rabin, Y.; Szleifer, I. Transport Rectification in Nanopores with Outer Membranes Modified with Surface Charges and Polyelectrolytes. *ACS Nano* **2013**, *7* (10), 9085–9097.
- (46) Tagliazucchi, M.; Calvo, E. J.; Szleifer, I. Molecular Theory of Chemically Modified Electrodes by Redox Polyelectrolytes under Equilibrium Conditions: Comparison with Experiment. *J. Phys. Chem.* C 2008, 112 (2), 458–471.
- (47) Tagliazucchi, M.; de la Cruz, M. O.; Szleifer, I. Self-Organization of Grafted Polyelectrolyte Layers *via* the Coupling of Chemical Equilibrium and Physical Interactions. *Proc. Natl. Acad. Sci. U. S. A.* **2010**, *107* (12), 5300–5305.
- (48) Tagliazucchi, M.; Peleg, O.; Kröger, M.; Rabin, Y.; Szleifer, I. Effect of Charge, Hydrophobicity, and Sequence of Nucleoporins on the Translocation of Model Particles through the Nuclear Pore Complex. *Proc. Natl. Acad. Sci. U. S. A.* **2013**, *110* (9), 3363–3368.
- (49) Tagliazucchi, M.; Li, X.; Olvera de la Cruz, M.; Szleifer, I. Self-Organized Polyelectrolyte End-Grafted Layers under Nanoconfinement. *ACS Nano* **2014**, *8* (10), 9998–10008.
- (50) Hehmeyer, O. J.; Arya, G.; Panagiotopoulos, A. Z.; Szleifer, I. Monte Carlo Simulation and Molecular Theory of Tethered Polyelectrolytes. *J. Chem. Phys.* **2007**, *126* (24), 244902.
- (51) Gong, P.; Wu, T.; Genzer, J.; Szleifer, I. Behavior of Surface-Anchored Poly(acrylic Acid) Brushes with Grafting Density Gradients

on Solid Substrates: 2. Theory. *Macromolecules* **2007**, 40 (24), 8765–8773.

(52) Wang, D.; Nap, R. J.; Lagzi, I.; Kowalczyk, B.; Han, S.; Grzybowski, B. A.; Szleifer, I. How and Why Nanoparticle's Curvature Regulates the Apparent pKa of the Coating Ligands. *J. Am. Chem. Soc.* **2011**, *133* (7), 2192–2197.